Theoretical and Applied Fracture Mechanics 16 (1991) 109–122
Elsevier

Fatigue crack growth rate in ferrite–martensite dual-phase steel

R.Y. Deng and Z.J. Ye

Institute of Mechanics, Academia Sinica, Beijing, People's Republic of China

An empirical study is made on the fatigue crack growth rate in ferrite–martensite dual-phase (FMDP) steel. Particular attention is given to the effect of ferrite content in the range of 24.2% to 41.5% where good fatigue resistance was found at 33.8%. Variations in ferrite content did not affect the crack growth rate da/dN when plotted against the effective stress intensity factor range ΔK_{eff} which was assumed to follow a linear relation with the crack tip stress intensity factor range ΔK. A high ΔK_{eff} corresponds to uniformly distributed small size ferrite and martensite. No other appreciable correlation could be related to the microstructure morphology of the FMDP steel. The closure stress intensity factor K_{cl}, however, is affected by the ferrite content with K_{cl}/K_{max} reaching a maximum value of 0.7. In general, crack growth followed the interphase between the martensite and ferrite.

Dividing the fatigue crack growth process into Stage I and II where the former would be highly sensitive to changes in ΔK and the latter would increase with ΔK depending on the $R = \sigma_{min}/\sigma_{max}$ ratio. The same data when correlated with the strain energy density factor range ΔS showed negligible dependence on mean stress or R ratio for Stage I crack growth. A parameter α involving the ratio of ultimate stress to yield stress, percent reduction of area and R is introduced for Stage II crack growth so that the da/dN data for different R would collapse onto a single curve with a narrow scatter band when plotted against $\alpha\Delta S$.

1. Introduction

Improved strength and ductility can create a two-phase microstructure in steel. This can be achieved by appropriate heat treatment [1–4]. Under repeated stresses, microscopic plasticity introduces nonhomogeneity in the dual-phase steel on account of the dissimilar physical/mechanical properties of the martensite and ferrite in addition to their size and distribution. These effects are reflected through the fatigue crack growth data which are analyzed in this work as the ferrite content and mean stress level are varied.

The data are generally represented by plots of da/dN against ΔK. Better correlation can be obtained by using the strain energy density factor range ΔS [5,6] that accounts for the mean stress effect. An empirical parameter α suggested in [7,8] is also used as a correction on ΔS or $\alpha\Delta S$ for representing crack growth rate data.

2. Description of heat treatment and fatigue tests

Special heat treatments are administered to create different ferrite contents in specimens which are notched for initiating cracks under cyclic loading. Crack propagation data are then taken by varying the mean stress level of the constant amplitude loading.

2.1. Heat treatment

Two types of heat treatments are given to the 16 MnR steel in rolled condition with 16 mm thickness so that the ferrite content and microstructure could be varied. The first set of specimens were heated at 780 °C, 810 °C and 850 °C in the two phase region; they are then quenched in brine and tempered at 200 °C. This batch is referred to A-1, A-2 and A-3 with the corresponding mechanical properties given in Table 1. Note that the martensite microhardness tends to reduce with the heat treatment temperature. The second batch labelled as B-1, B-2 and B-3 in Table 1 were heated at 1200 °C for diffuse annealing. They were subsequently heated at 930 °C and then cooled in brine, air and furnace. All of them were heated again to 810 °C followed by quenching in brine and tempering at 200 °C. Shown in Figs. 1(a), 1(b) and 1(c) are, respectively, the microstructure of specimens B-1, B-2

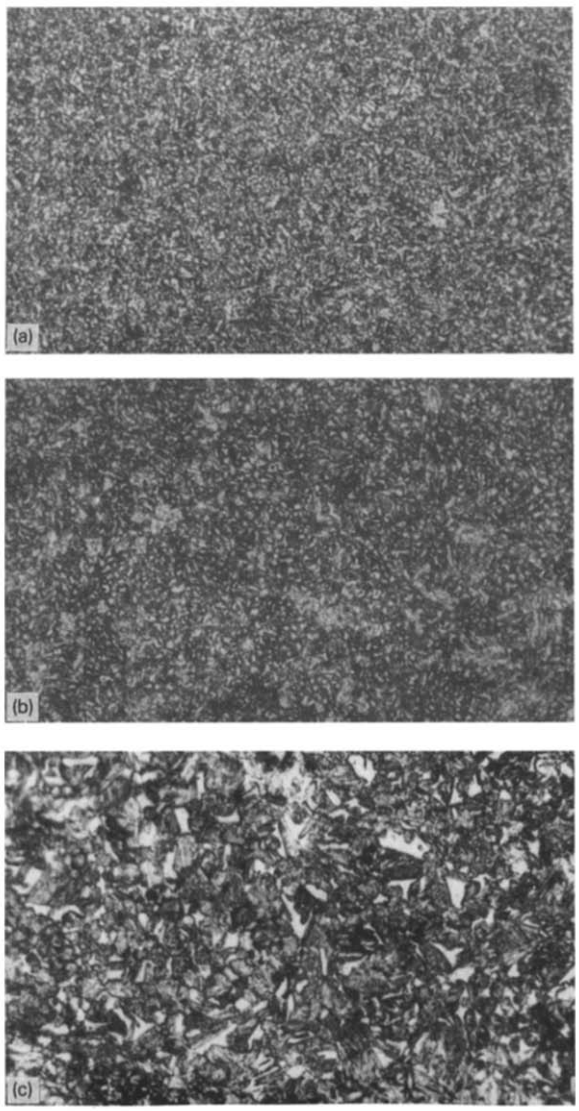

Fig. 1. Microstructure (200×) of dual-phase steel with different heat treatments: specimens (a) B-1; (b) B-2; and (c) B-3.

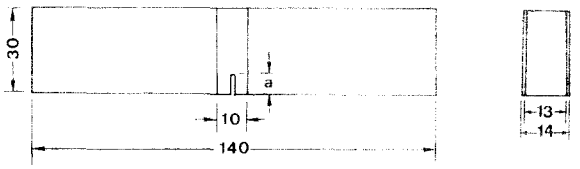

Fig. 2. Schematic of FMDP steel notched specimen (dimensions in mm).

and B-3 magnified 200 times. Increase in the coarseness of the microstructure is clearly shown. The ferrite contents were measured by application of Quantiment 520 phase analysis equipment.

2.2. Specimen configuration and load

The dimensions of the test specimen are 140 mm × 30 mm × 13 mm as shown in Fig. 2. It contains an initial notch of length a at the center and is subjected to three-point bending repeated cyclically at constant amplitudes of $\Delta P = 700$ kgf and 910 kgf with a frequency of 90 Hz under room temperature condition. Two values of $R = \sigma_{min}/\sigma_{max} = 0.3$ and 0.7 are used.

2.3. Crack initiation

During the early stage of cyclic loading with $R = 0.3$, slip lines appeared near the notch and they gradually develop into microcracks as the load cycles are increased. Figure 3 shows that most of the microcracks initiated at the interphase between the ferrite and martensite. The microcracks grew progressively and coalesced to form a main crack when $\Delta P = 700$ kgf. At $\Delta P = 910$ kgf, several microcracks developed near the

Table 1
Mechanical properties of ferrite–martensite steel

Specimen type	Young's modulus $E \times 10^5$ (MPa)	Hardening exponent n	Elongation %	Reduction in area %	Yield stress (0.2% offset) σ_{ys} (MPa)	Ultimate stress σ_{ul} (MPa)	Ferrite content %	Martensite microhardness HV
As rolled	2.48	0.17	16.7	68.7	367	545	–	–
A-1	1.82	0.12	10.3	43.1	603	930	41.8	342
A-2	1.52	0.09	11.2	44.9	720	984	33.8	241
A-3	1.94	0.08	7.9	42.5	755	1021	24.2	196
B-1	2.05	0.11	14.4	46.1	692	966	29.5	229
B-2	2.07	0.12	14.2	46.7	542	880	32.7	262
B-3	2.00	0.14	15.1	47.5	535	877	33.5	252

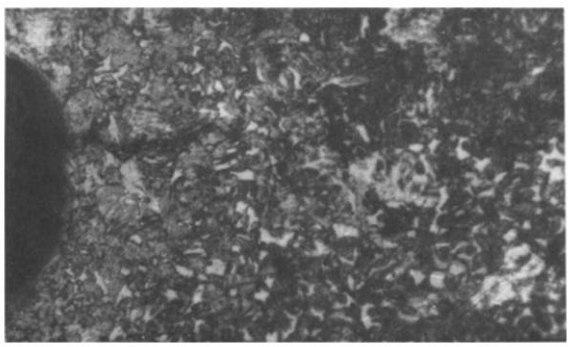

Fig. 3. Microcracks initiated at interphase of ferrite and martensite (200×).

notch about the same time. As they reached a length of approximately 0.3 to 0.6 mm, the leading one would take off while the others remain behind. The crack initiation life N_0 for the FMDP steel is larger than the 16 MnR steel in its rolled state. The largest initiation life was obtained for specimen B-1 corresponding to a dual-phase steel heated at 930 °C and then cooled in brine. Increase in N_0 is about an order of magnitude more than the 16 MnR rolled steel. The results are summarized in Table 2.

3. Correlation of crack growth rate

Fatigue crack growth data are usually presented by plotting the rate da/dN as a function of a parameter that represents the range of the local stress intensity or equivalent quantity. One of the quantities to be considered is the threshold stress intensity range ΔK_{th} corresponding to 10^6 cycles of loading with a crack growth increment of not more than 0.1 mm; it is defined as

$$\Delta K_{eff} = K_{max} - K_{cl} \quad (1)$$

where K_{cl} is crack closure stress intensity factor [9,10]. Shown in Table 3 are values of ΔK_{th} and K_{cl} for the different specimens. For $R = 0.3$, the highest and lowest ΔK_{th} correspond, respectively, to specimen B-1 with 29.5% ferrite and A-1 with 41.5% ferrite. Variations of ΔK_{th} with ferrite content are not as pronounced for R = 0.7.

Table 2
Crack initiation life

Specimen type	Initiation life $N_0 \times 10^5$ (cycles)	
	$\Delta P = 700$ kgf	$\Delta P = 910$ kgf
As rolled	1.10	0.43
A-1	4.23	1.22
A-2	6.69	3.74
A-3	5.99	2.98
B-1	71.80	4.86
B-2	24.80	4.28
B-3	22.51	3.92

Table 3
Stress intensity factor: threshold and closure

Specimen type	Threshold ΔK_{th} (MPa$\sqrt{m}$)		Closure K_{cl} (MPa$\sqrt{m}$)
	$R = 0.3$	$R = 0.7$	
As rolled	6.85	4.20	5.37
A-1	7.90	4.73	6.60
A-2	8.97	3.92	8.93
A-3	8.34	4.20	7.72
B-1	10.30	6.60	8.1
B-2	9.41	5.51	7.9
B-3	9.25	5.45	8.1

3.1. Stress intensity factor range

Plotted in Fig. 4(a) are $\log da/dN$ versus $\log \Delta K$ for $R = 0.3$ where four different values of ΔK_{th} are obtained as given in Table 3. A slight variation in ΔK would yield large changes in da/dN. The values of ΔK_{th} were measured by using load decrease by degrees with ΔK value. This regime is referred to as Stage I crack propagation. Application of eq. (1) and the formula

$$\frac{da}{dN} = 4.2141 \times 10^{-17} (\Delta K_{eff})^{9.1026} \quad (2)$$

The same data could be represented by a single curve with a correlation coefficient of 0.9315 as shown in Fig. 4(b). Corrections for the crack closure effect tends to increase with decreasing ΔK. They are shown in Fig. 5 and are in agreement with the results in [11–13]. A maximum of $K_{cl}/K_{max} = 0.7$ is obtained for the A-2 specimen with 33.8% ferrite which has the lowest crack growth rate, Fig. 4(a). Similarly, the ΔK_{th} values for specimens B-1, B-2 and B-3 in Table 3 for $R = 0.3$ and 0.7 can be obtained by decreasing the applied load amplitude. The stage I crack propa-

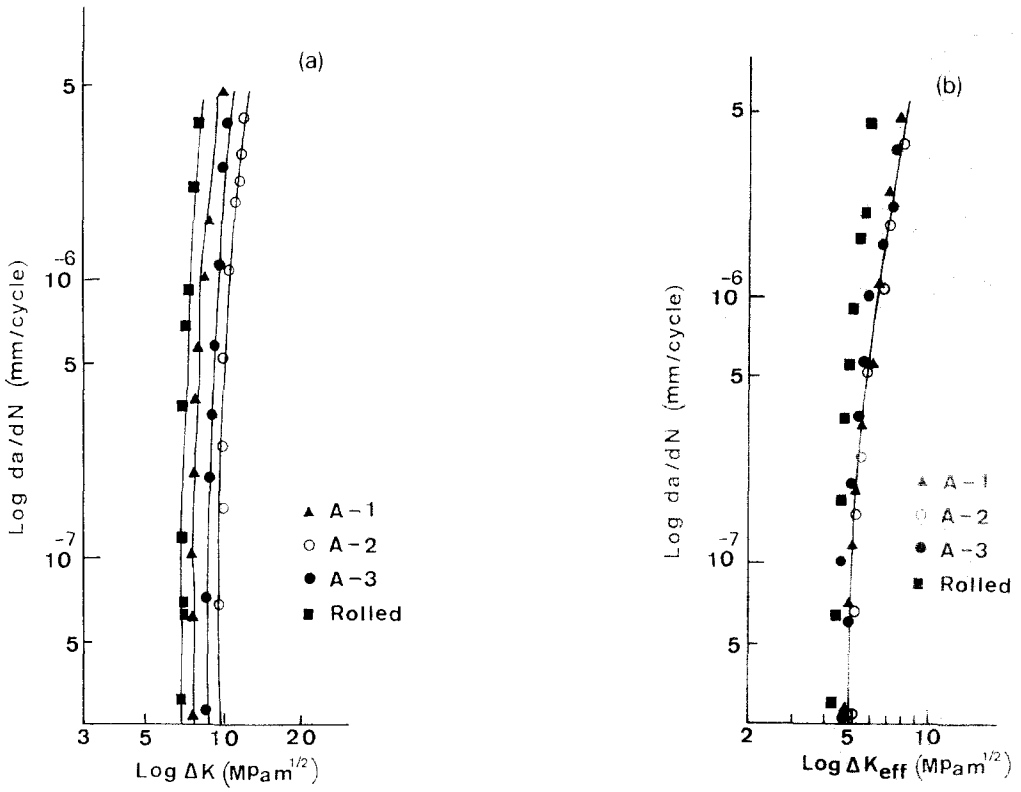

Fig. 4. Stage I crack propagation near threshold at $R = 0.3$ for specimens A-1, A-2 and A-3.

gation is shown, respectively, in Figs. 6(a) and 6(b) on plots of da/dN versus ΔK. The data scatter, however, did not improve when ΔK_{eff} is used instead of ΔK. This is shown in Fig. 6(c) for

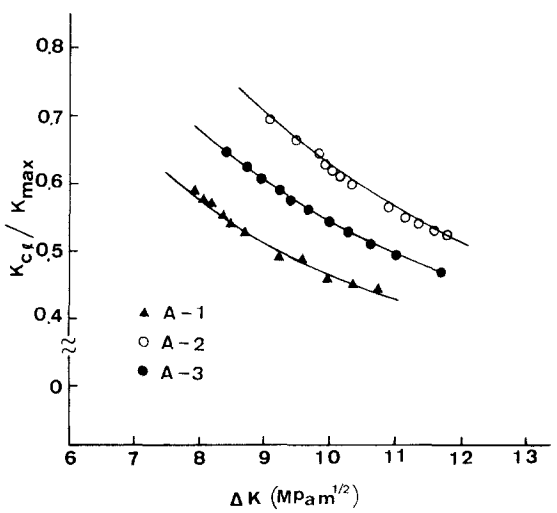

Fig. 5. Normalized Stage I crack closure intensity factor versus crack tip intensity range for specimens A-1, A-2 and A-3 with $R = 0.3$.

$R = 0.3$. Largest $(\Delta K_{eff})_{th}$ value corresponds to specimen B-1 while K_{cl} remains unchanged for the three cases. A straight line relationship is obtained in Fig. 7 when ΔK_{eff} is plotted against ΔK:

$$\Delta K_{eff} = -27.8512 + 1.4783\ \Delta K \tag{3}$$

The correlation coefficient is 0.9898.

Generally speaking, at a given ΔK level, a lower ΔK_{th} would correspond to higher crack growth as shown by the data in Figs. 6(a)–6(c). This is consistent with the results in Fig. 8 that plots K_{cl}/K_{max} against ΔK because

$$\Delta K = K_{max}(1 - R) \tag{4}$$

where $R = \sigma_{min}/\sigma_{max}$. Applying eq. (1) to the condition at threshold, there results

$$(K_{max})_{th} = K_{cl} + (\Delta K_{eff})_{th} \tag{5}$$

Because $(\Delta K_{eff})_{th}$ is largest for B-1 in Fig. 6(c), the same holds for $(K_{max})_{th}$ from eq. (5) as K_{cl} does not change. The ratio K_{cl}/K_{max} would therefore be the smallest for B-1 as shown in Fig. 8. It is change in the microstructure of the dual-

phase steel that alters the deviations in crack growth characteristics. Crack closure has been attributed to fracture surface roughness [14] at room temperature and to the austenite grain size [15,16]. These, however, are only qualitative observations. How does crack closure affect crack

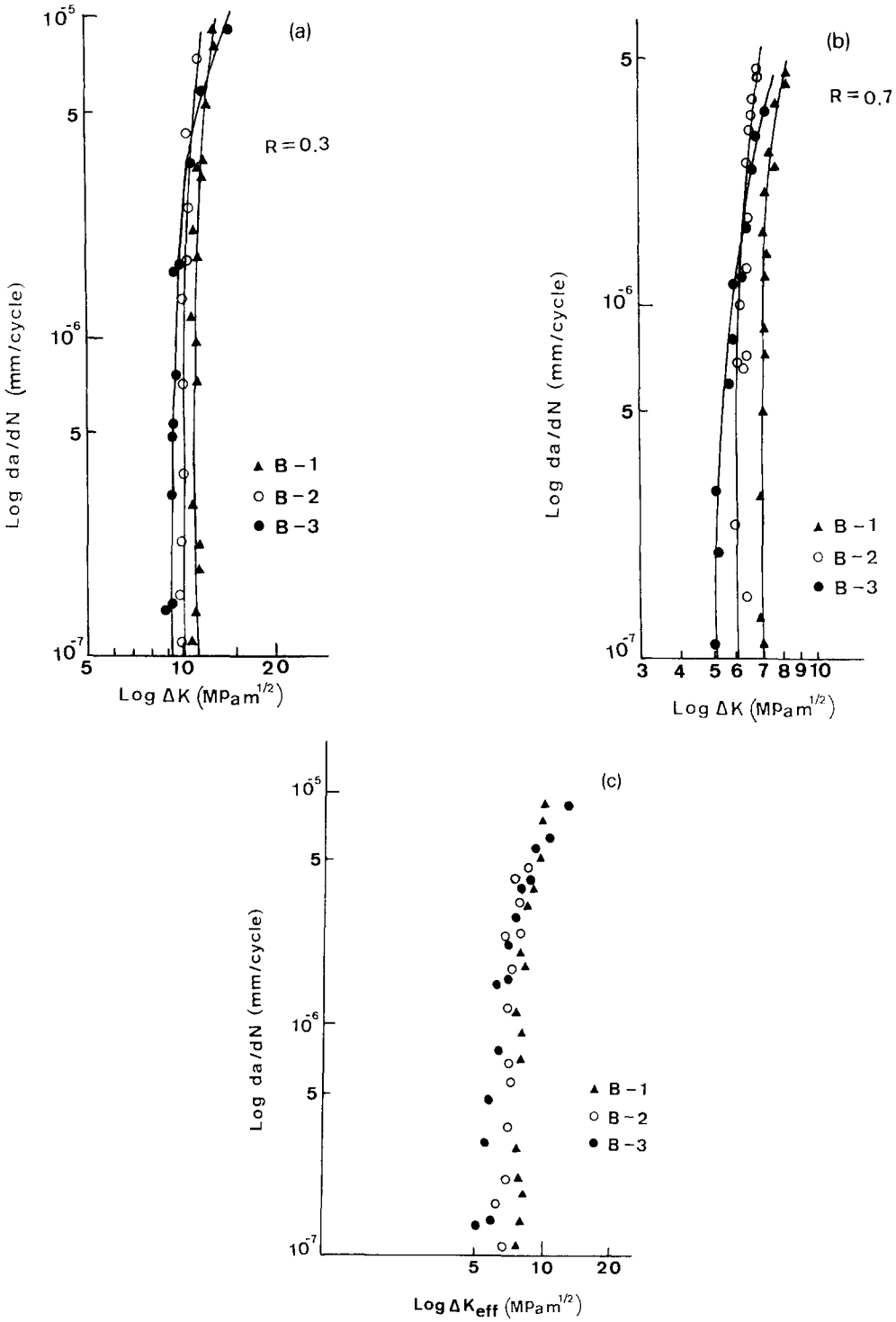

Fig. 6. Stage I crack propagation near threshold for specimens B-1, B-2 and B-3.

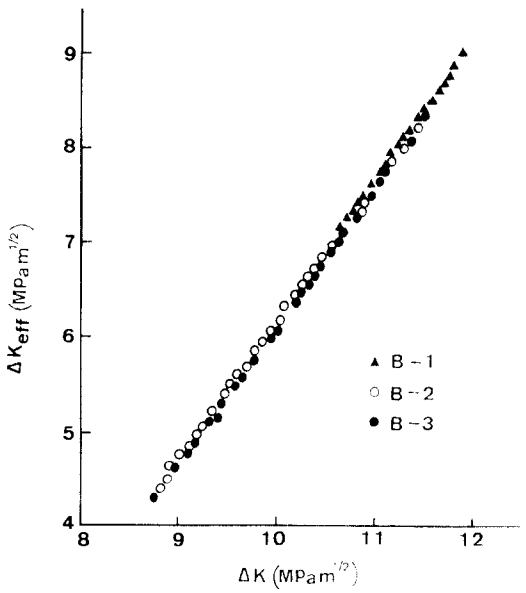

Fig. 7. Stage I effective versus crack tip stress intensity factor range for specimens B-1, B-2 and B-3 with $R = 0.3$.

growth retardation is still not very clear. Recent work has shown that the crack opening displacement and closure do not correlate well [17] with observed fatigue damage data. No conclusive remarks could be made from the empirical approach except to show that the influence of material microstructure on crack growth.

Stage II crack growth data for specimens B-1, B-2 and B-3 are shown in Fig. 9(a) for $R = 0.3$ and Fig. 9(b) for $R = 0.7$. Deviations among the

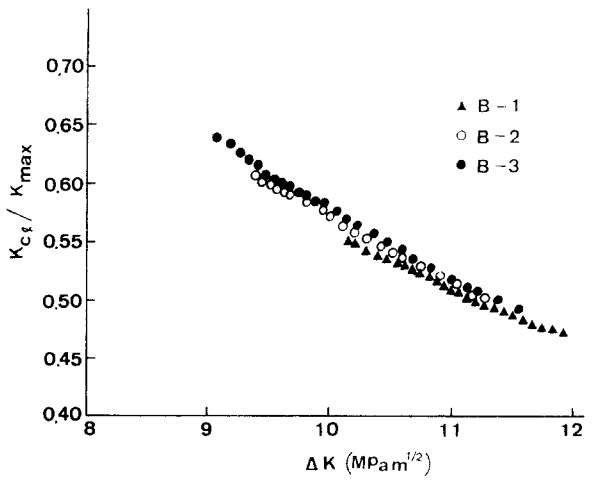

Fig. 8. Normalized Stage I crack closure stress intensity factor versus crack tip stress intensity factor range for specimens B-1, B-2 and B-3 with $R = 0.3$.

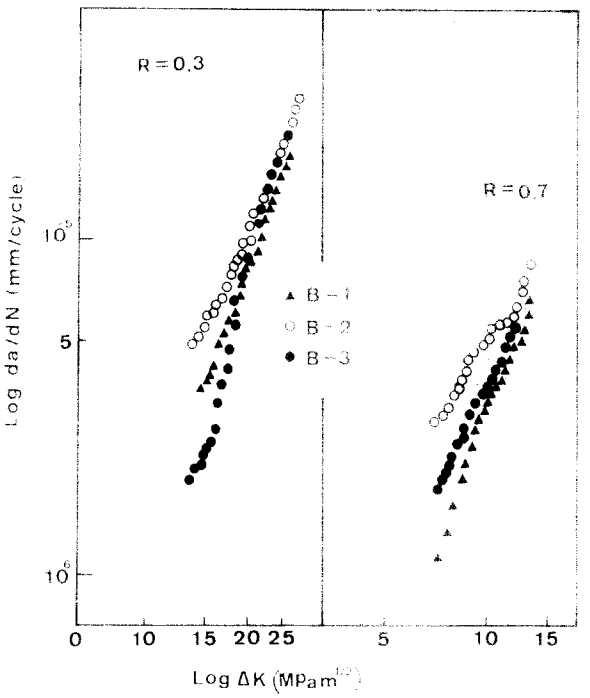

Fig. 9. Stage II crack growth rate for specimens B-1, B-2 and B-3 with $R = 0.3$ and 0.7.

curves due to differences in material microstructure are large for low ΔK but they tend to diminish at $\Delta K = 22$ MPa$\sqrt{\text{m}}$ for $R = 0.3$ and $\Delta K = 11.8$ MPa$\sqrt{\text{m}}$ for $R = 0.7$.

3.2. Strain energy density factor range

One of the obvious deficiencies of da/dN versus ΔK plots is that the mean stress level is not accounted for. Data would tend to scatter as different R ratios are used. The strain energy density factor range ΔS [5–8] includes the mean stress effect and yields better correlation with fatigue data. Proposed in [7,8] were a way to best fit the fatigue data by assuming that da/dN is a function of ΔS or $\alpha \Delta S$:

$$\frac{da}{dN} = f(\Delta S) \quad \text{or} \quad f(\alpha \Delta S) \tag{6}$$

A regression technique was developed to best fit the experimental data. In eq. (6), α is a parameter given by

$$\alpha = \frac{1 + R}{1 + R\beta^2} \tag{7}$$

in which

$$\beta = \frac{\sigma_{ul}}{\sigma_{ys}}(1 + \%RA) \tag{8}$$

Values of σ_{ul}, σ_{ys} and %RA for the FMDP steel specimens are given in Table 1. According to the strain energy density criterion [5,6], the strain energy density factor range is given by

$$\Delta S = S_{max} - S_{min} \tag{9}$$

For a Mode I crack problem, ΔS can be written as

$$\Delta S = \frac{(1+\nu)(1-2\nu)}{2\pi E}\left(\frac{1+R}{1-R}\right)\Delta K^2 \tag{10}$$

with $\nu = 0.3$ for steel and E can be found in Table 1. Without going into details, the same fatigue data as given in Tables 4 and 5 will be presented using ΔS and compared to those using ΔK for the specimens B-1, B-2 and B-3 with R = 0.3 and 0.7.

Table 4
Crack growth data for specimens B-1, B-2 and B-3 with $R = 0.3$

Specimen B-1		Specimen B-2		Specimen B-3	
a (mm)	N $\times 10^3$ (cycle)	a (mm)	N $\times 10^3$ (cycle)	a (mm)	N $\times 10^3$ (cycle)
7.97	196,274	8.00	197,279	8.05	198,794
8.27	196,317	8.30	197,315	8.25	198,865
8.57	196,354	8.60	197,347	8.55	198,976
8.87	196,400	8.90	197,389	8.88	199,117
9.17	196,457	9.20	197,430	9.05	199,242
9.47	196,520	9.50	197,477	9.25	199,327
9.77	196,583	9.80	197,524	9.45	199,402
10.07	196,645	10.10	197,571	9.65	199,483
10.37	196,705	10.40	197,610	9.85	199,557
10.67	196,758	10.73	197,659	10.08	199,622
10.97	196,810	11.04	197,695	10.25	199,673
11.27	196,869	11.30	197,727	10.45	199,726
11.57	196,903	11.60	197,760	10.65	199,777
11.87	196,941	11.90	197,791	10.85	199,816
12.17	196,973	12.20	197,819	11.05	199,862
12.47	197,004	12.50	197,845	11.40	199,914
12.82	197,035	12.80	197,868	11.73	199,967
13.17	197,064	13.10	197,895	11.95	199,998
13.47	197,088	13.40	197,915	12.25	200,937
13.77	197,113	13.70	197,937	12.65	200,074
14.09	197,149	14.00	197,958	12.85	200,091
14.37	197,174	14.30	197,976	13.18	200,119
14.67	197,192	14.63	198,000	13.45	200,138
		14.90	198,011	13.75	200,157
		15.20	198,025	14.05	200,177
		15.50	198,040	14.35	200,195
				14.65	200,213
				14.95	200,248

Table 5
Crack growth data for specimens B-1, B-2 and B-3 with R = 0.7

Specimen B-1		Specimen B-2		Specimen B-3	
a (mm)	N $\times 10^3$ (cycle)	a (mm)	N $\times 10^3$ (cycle)	a (mm)	N $\times 10^3$ (cycle)
8.93	200,267	8.00	202,715	7.54	204,229
9.13	200,465	8.30	202,727	7.65	204,350
9.33	200,733	8.60	202,760	7.89	204,463
9.56	201,005	8.90	202,785	8.05	204,585
9.73	201,212	9.20	202,868	8.25	204,689
10.10	201,327	9.50	202,934	8.55	204,835
10.46	201,419	9.80	203,008	8.95	204,993
10.76	201,512	10.10	203,080	9.25	205,105
11.36	201,767	10.40	203,160	9.55	205,210
11.66	201,836	10.70	203,222	9.85	205,359
11.96	201,921	11.00	203,291	10.15	205,479
12.26	202,012	11.30	203,361	10.45	205,595
12.56	202,098	11.70	203,420	10.75	205,714
12.86	202,173	12.00	203,480	11.05	205,818
13.16	202,253	12.30	203,530	11.35	205,912
13.46	202,336	12.60	203,597	11.65	206,007
13.76	202,402	12.90	203,662	11.95	206,095
14.06	202,467	13.20	203,720	12.25	206,183
14.36	202,521	13.50	203,790	12.55	206,260
14.56	202,587	13.80	203,855	12.85	206,324
14.86	202,635	14.20	203,919	13.18	206,401
15.16	202,685	14.60	203,978	13.45	206,457
		15.00	204,035	13.75	206,513
				14.05	206,571

Stage I. Exhibited in Figs. 10(a), 11(a) and 12(a) would be crack growth rate plots using ΔK while those in Figs. 10(b), 11(b) and 12(b) would be based on ΔS for the Stage I regime where the cracks grow relatively slow. The general trends of the curves for specimens B-1, B-2 and B-3 are similar where the data scatter caused by the difference in R = 0.3 and 0.7 is significant when using ΔK and diminishes when using ΔS. This observation was also made in [6] for other metal alloys.

Stage II. Even better correlation is obtained if α in eq. (7) is included [7,8]. Particularly noticeable is the data in Figs. 13(a) and 13(b) for the B-1 specimen. The two curves based on ΔK in Fig. 13(a) merged into one when they are represented

by $\alpha\Delta S$ in Fig. 13(b). Similar tendencies can be seen from the results in Figs. 14(a) and 14(b) for specimen B-2 and Figs. 15(a) and 15(b) for specimen B-3.

4. Ductility and crack path

A phase contact microscope is used to observe the distorted zone in linear dimension of ω next to the main crack surface. This is shown in Fig. 16 where the slip bands appear as wavy lines and microcracks around the main crack show up as darker lines. Measurements are taken at threshold and Stage II crack growth in terms of the parameter

$$\Omega = \frac{\omega}{(K_{max}/\sigma_{ys})^2} \tag{11}$$

Their values are summarized in Table 6 for $R = 0.3$ and 0.7 where Ω_{th} stands for Ω at the threshold condition. A large Ω corresponds to more distortion of the material around the crack which would presumably translate to more plastic deformation or ductility. It increases with the ferrite content that is assumed to have plastic flow. Table 6 also shows that Ω_{th} or Ω decreases with increasing R as it would be expected on physical ground.

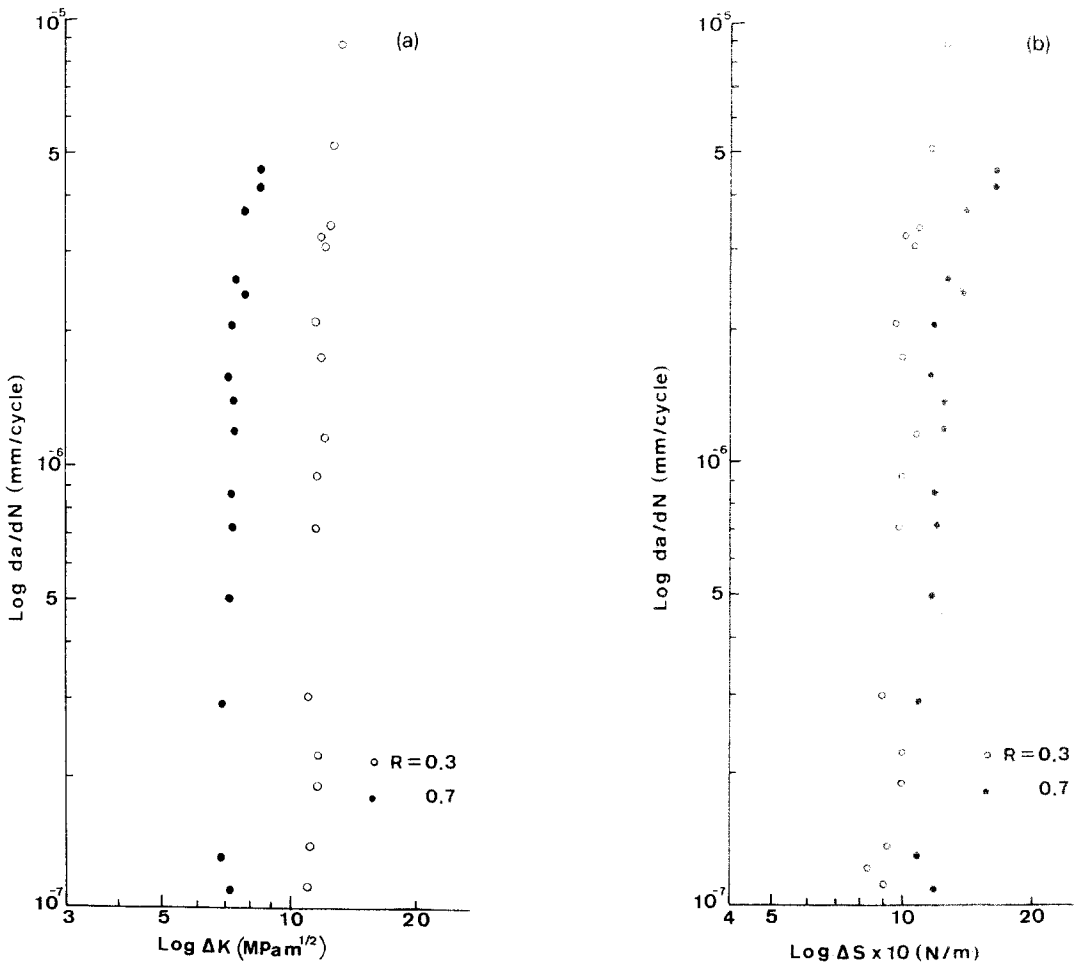

Fig. 10. Stage I crack growth rate against ΔK and ΔS for B-1 specimen with $R = 0.3$ and 0.7.

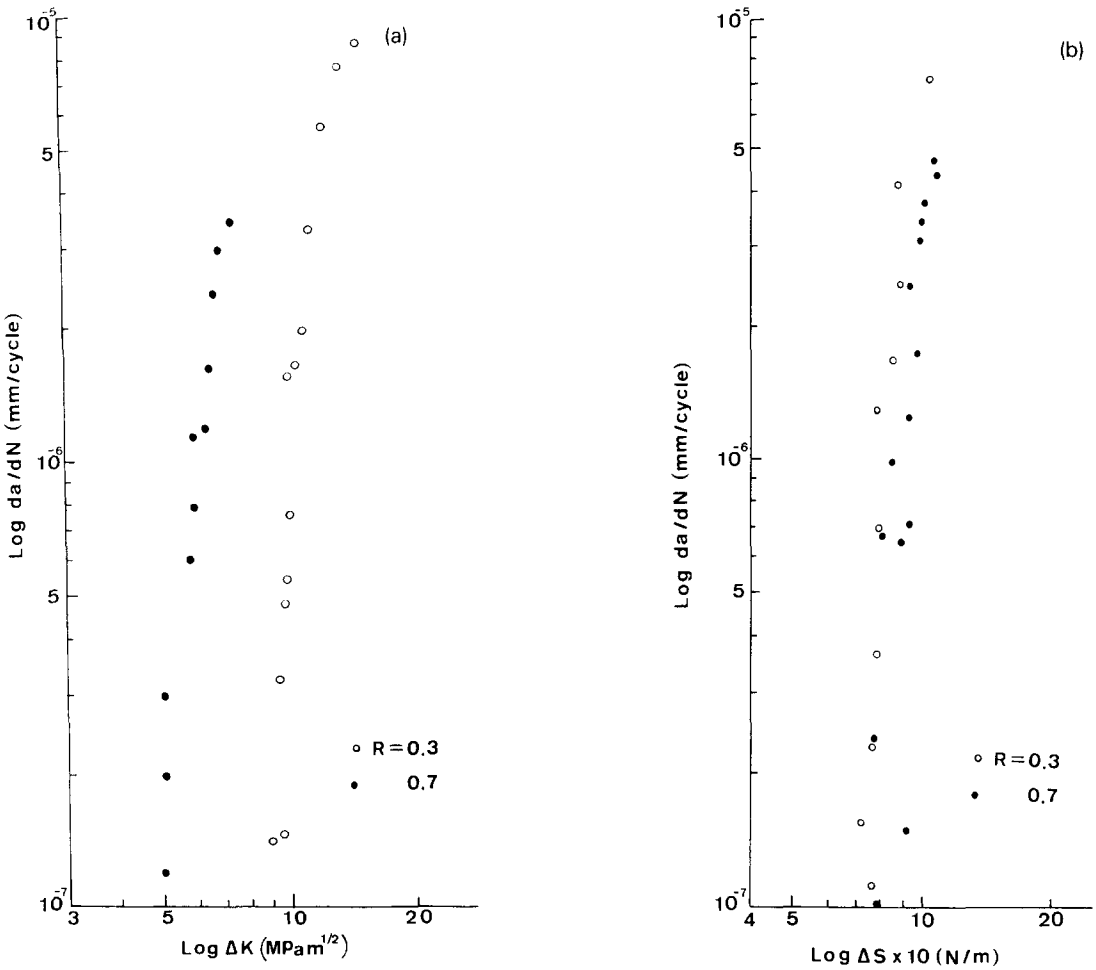

Fig. 11. Stage I crack growth rate against ΔK and ΔS for B-2 specimen with $R = 0.3$ and 0.7.

Electron microphoto in Fig. 17 shows that main crack follows the interphase boundary between the ferrite and martensite. The fracture surface is predominantly quasi-cleavage appearing as martensite platelets while cleavage corresponds to the ferrite shown in the square region identified in Fig. 18 by an arrow. Observed at threshold are small facets about the size of the original austenite grains and parallel striations on the cleavage plateau.

5. Conclusions

Appropriate heat treatment can be applied to the 16 MnR steel to introduce ferrite and martensite making the steel a two-phase material that would yield high strength, good ductility and better resistance to fatigue. Based on the empirical study, the following conclusions could be made:

- Two sets of specimens were made subjecting them to different heat treatments. The specimen labelled as B-1 was superior to others.
- Ferrite contents were found to affect the crack growth rates correlated in terms of stress intensity factor ranges identified with threshold and crack closure.
- The strain energy density factor range gave better correlation than the stress intensity factor range where data for different mean stresses collapsed into a single curve where the scatter is limited.
- Local distortion of the material next to the main crack could be measured and introduced into an empirical parameter. It can be used to rank the material ductility as other physical parameters are varied.

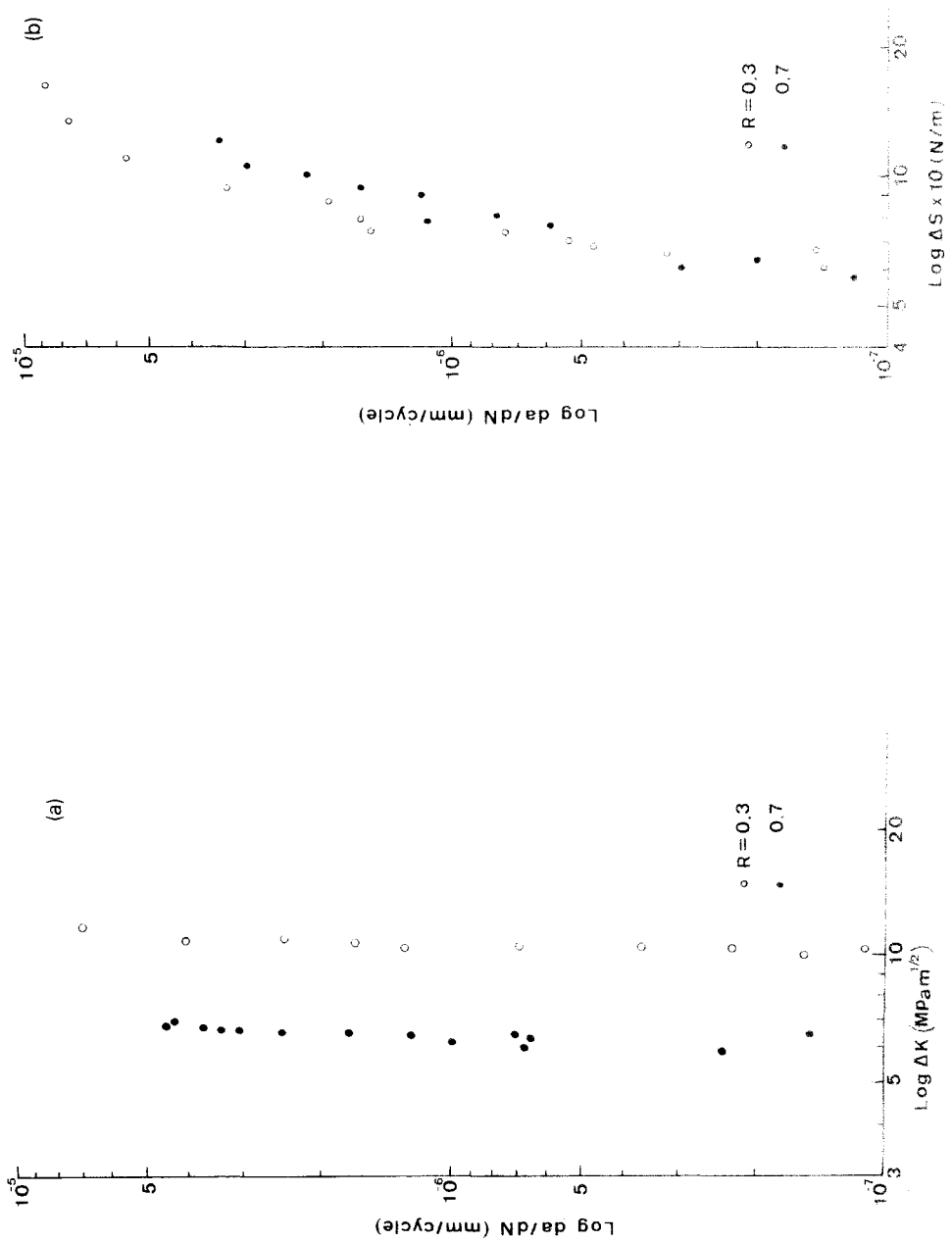

Fig. 12. Stage I crack growth rate against ΔK and ΔS for B-3 specimen with $R = 0.3$ and 0.7.

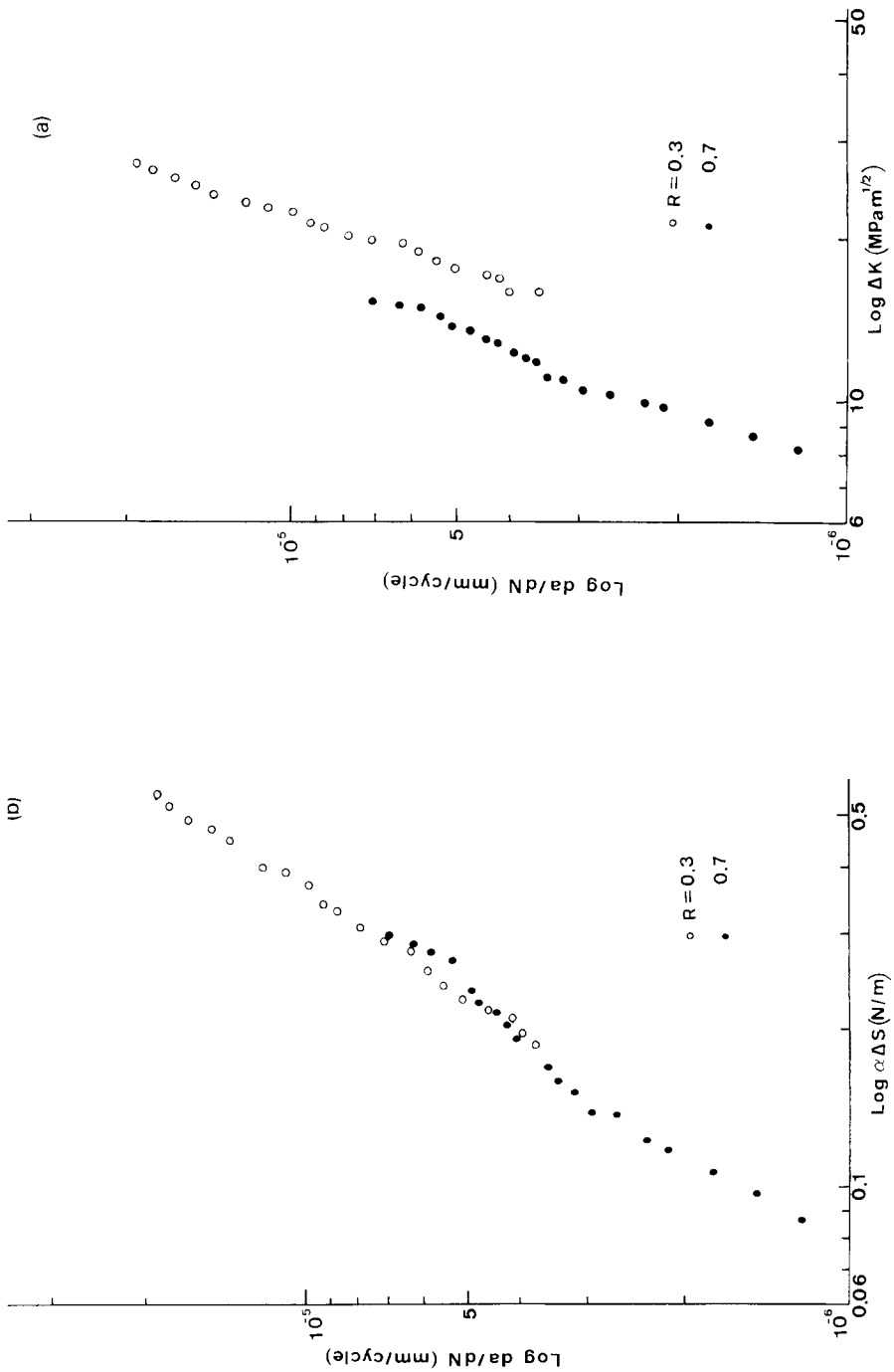

Fig. 13. Stage II crack growth rate against ΔK and $\alpha\Delta S$ for B-1 specimen with $R = 0.3$ and 0.7.

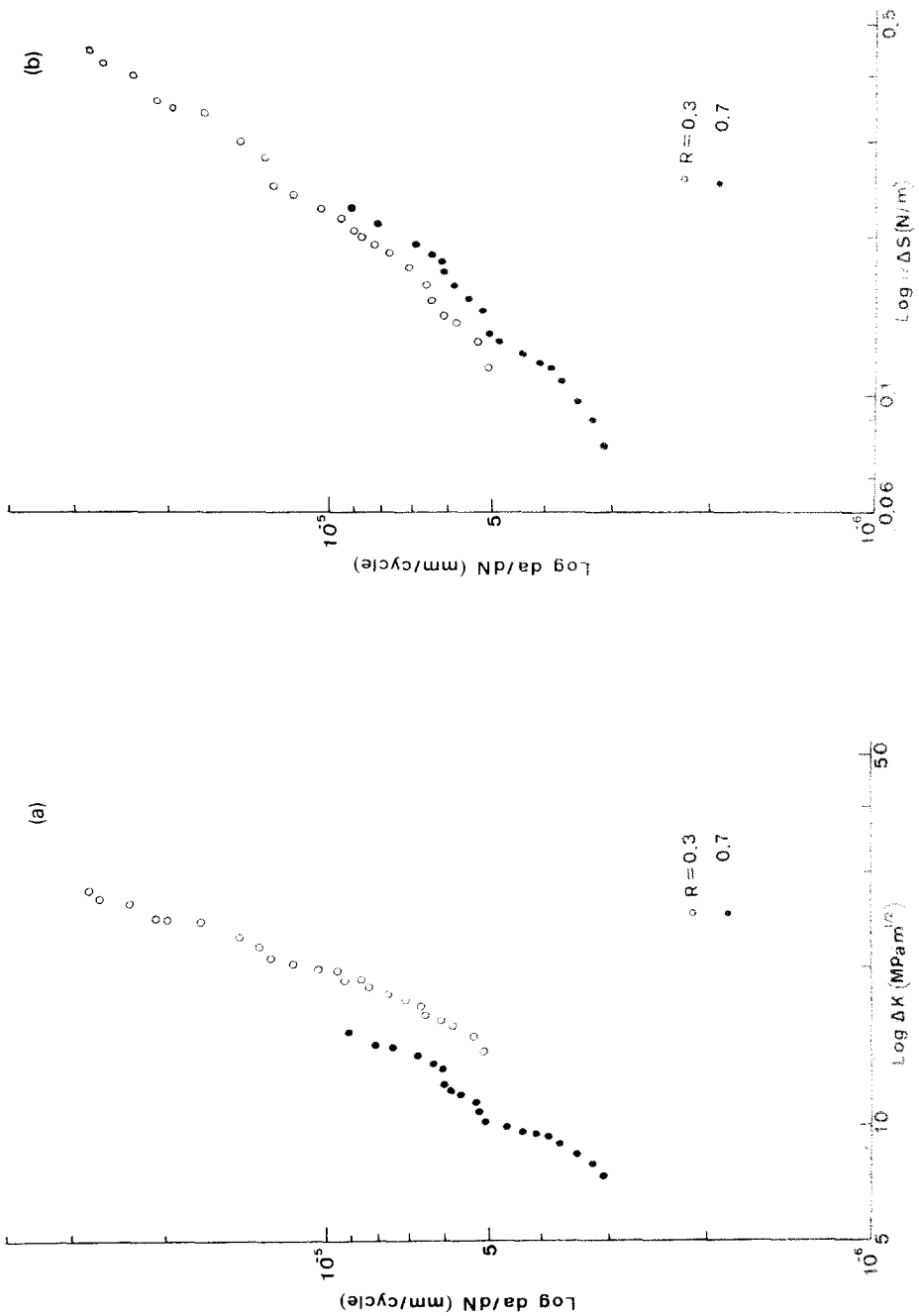

Fig. 14. Stage II crack growth rate against ΔK and $\sigma\Delta S$ for B-2 specimen with $R = 0.3$ and 0.7.

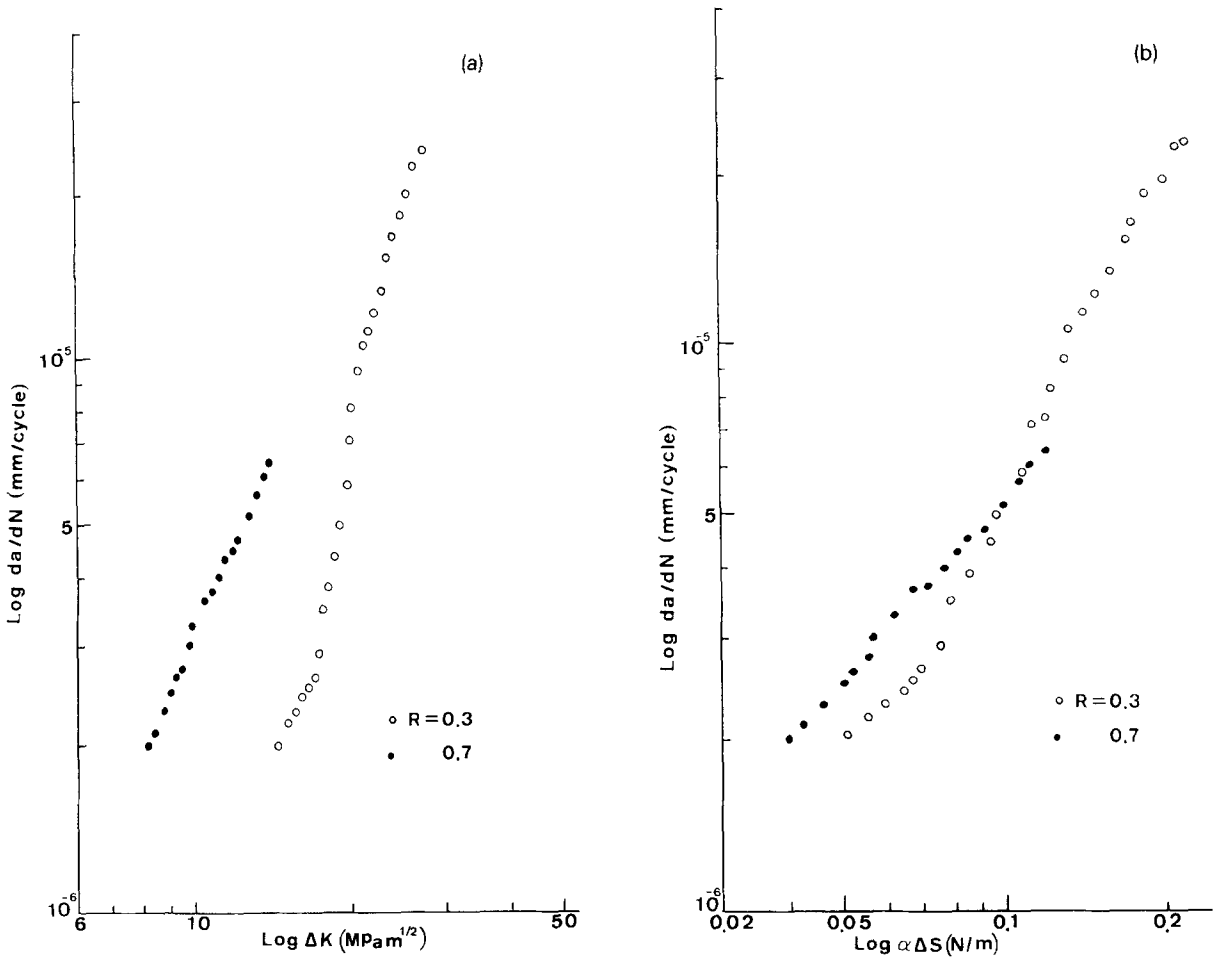

Fig. 15. Stage II crack growth rate against ΔK and $\alpha\Delta S$ for B-3 specimen with $R = 0.3$ and 0.7.

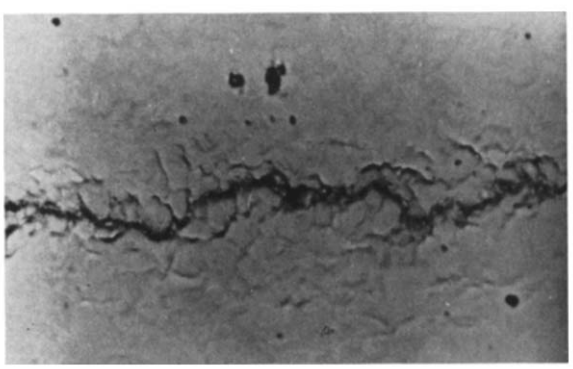

Fig. 16. Microcracks emanating from both sides of main crack (300×).

Table 6
Distortion factor measuring ductility of FMDP steel

Specimen type	Ω_{th} (threshold)		Ω (Stage II)	
	$R = 0.3$	$R = 0.7$	$R = 0.3$	$R = 0.7$
A-1	0.0502	–	0.0450	–
A-2	0.0284	–	0.0109	–
A-3	0.0153	–	0.0088	–
B-1	0.0307	0.0060	0.0077	0.0032
B-2	0.0305	0.0058	0.0078	0.0031
B-3	0.0310	0.0062	0.0084	0.0034

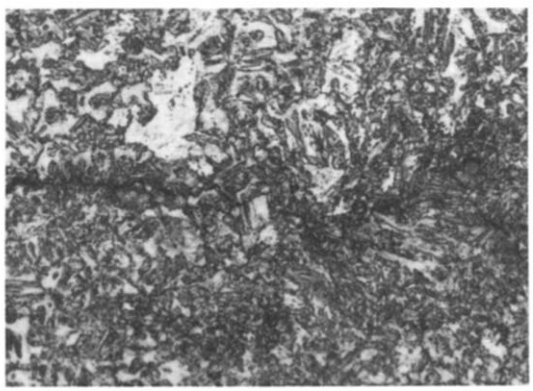

Fig. 17. Crack propagation path (400×).

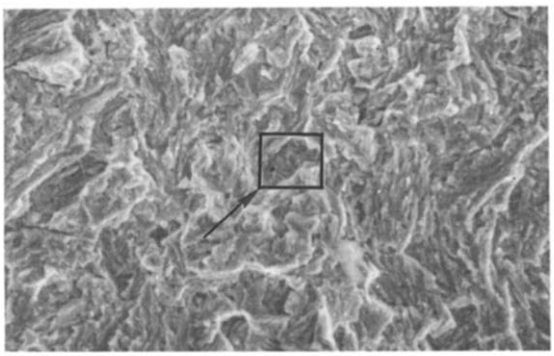

Fig. 18. Fracture morphology near threshold: quasi-cleavage and cleavage (800×).

Acknowledgements

This work was sponsored by the National Nature Science Foundation in the People's Republic of China.

References

[1] M.S. Rashid, GM980 X-A unique high strength sheet steel with superior formability, *SAE Trans. 85* (1976) 938–949.

[2] R.G. Davies, The deformation behavior of a vanadium-strengthened dual phase steel, *Metall. Trans. 7A* (1978) 41–52.

[3] H. Suzuki and A.J. McEvily, Microstructural effects on fatigue crack growth in a low carbon steel, *Metall. Trans. 10A* (1979) 475–484.

[4] T. Ishchara, Microstructural effects of fatigue crack growth in a two-phase steel, *J. Mater. Sci. 18* (1983) 103–108.

[5] G.C. Sih and B. Barthelemy, Mixed mode fatigue crack growth predictions, *Int. J. Eng. Fract. Mech. 13* (1980) 439–451.

[6] G.C. Sih, Fracture mechanics of engineering structural components, in *Fracture Mechanics Technology*, edited by G.C. Sih and L. Faria (Martinus Nijhoff: Dordrecht, The Netherlands, 1984) pp. 35–101.

[7] R. Badaliance, Application of strain energy density factor to fatigue crack growth analysis, *Int. J. Eng. Fract. Mech. 13* (1980) (3).

[8] R. Badaliance, A fatigue crack growth theory based on strain energy density, *Proc. Symposium on Absorbed Specific Energy Strain Energy Density*, edited by G.C. Sih, E. Czoboly and F. Gillemot, Budapest, Hungary, September 1980.

[9] R.Y. Deng and Y.F. Ma, Fatigue crack propagation near threshold in 15 MnVN steel, *Mechanical Strength 1* (1982) 22–28.

[10] R.Y. Deng and A.H. Zhou, Slow propagation of fatigue crack near threshold, *Acta Metall. Sinica 2A* (6) (1989) 439–443.

[11] V.B. Dutta, S. Suresh and R.O. Ritchie, Fatigue crack propagation in dual-phase steels: effects of ferrite-martensitic microstructures on crack path morphology, *Metall. Trans. 15A* (1984) 1193–1202.

[12] G.T. Gray, III, J.C. Williams and A.W. Thompson, Roughness-induced crack closure: an explanation for microstructurally sensitive fatigue crack growth, *Metall. Trans. 14A* (1983) 421–431.

[13] W.W. Gerberich, W. Yu and K. Esaklul, Fatigue threshold studies in Fe, Fe-Si and HSLA steel: part 1. Effect of strength and surface asperities on closure, *Metall. Trans. 15A* (1984) 875–888.

[14] S.Suresh, G.F. Zamiski and R.O. Ritchie, Oxide-induced crack closure: an explanation for near threshold corrosion fatigue crack growth behavior, *Metall. Trans 12A* (1981) 1435–1443.

[15] S. Suresh and R.O. Ritchie, A geometric model for fatigue crack closure induced by fracture surface roughness, *Metall. Trans. 13A* (1982) 1627–1631.

[16] R.Y. Deng, G.Q. Yu and H. Li, Effect of grain size on slow fatigue crack propagation and plastic deformation near crack tip, *Theoret. Appl. Fract. Mech. 7* (1) (1987) 37–40.

[17] G.C. Sih and D.Y. Jeong, Fatigue and load sequence effect ranked by critical available energy density, *Theoret. Appl. Fract. Mech. 14* (2) (1990) 141–151.